Cell Reports

Article

Rapid and reversible control of human metabolism by individual sleep states

Graphical abstract

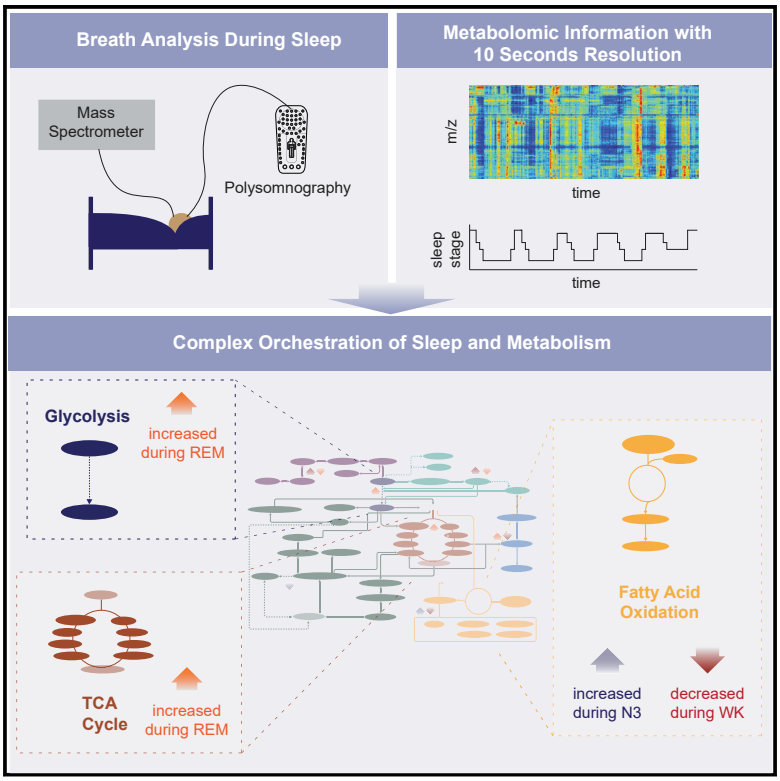

Highlights

- Sleep states regulate more than 50% of all metabolite features detected in human breath
- Major pathways are up- or downregulated during wake, SWS, and REM sleep
- Sleep-regulated pathways show stepwise logic across different sleep stages

Authors

Nora Nowak, Thomas Gaisl, Djordje Miladinovic, ..., Pablo Sinues, Steven A. Brown, Malcolm Kohler

Correspondence

steven.brown@pharma.uzh.ch (S.A.B.), malcolm.kohler@usz.ch (M.K.)

In brief

Measuring almost 2,000 metabolite features in breath every 10 s across a night of sleep, Nowak et al. demonstrate major pathways up- or downregulated during wake, slow-wave sleep, and rapid eye movement sleep. This control of metabolism by vigilance state is likely important in optimizing metabolic circuits for human health.

Nowak et al., 2021, Cell Reports *37*, 109903
October 26, 2021
https://doi.org/10.1016/j.celrep.2021.109903

CellPress

Cell Reports

CellPress
OPEN ACCESS

Article

Rapid and reversible control of human metabolism by individual sleep states

Nora Nowak,[1,2,6] Thomas Gaisl,[2] Djordje Miladinovic,[3] Ricards Marcinkevics,[3] Martin Osswald,[2] Stefan Bauer,[3] Joachim Buhmann,[3] Renato Zenobi,[1] Pablo Sinues,[4,5] Steven A. Brown,[6,*] and Malcolm Kohler[2,7,*]

[1]Department of Chemistry and Applied Biosciences, ETH Zurich, Zurich 8093, Switzerland
[2]Department of Pulmonology, University Hospital Zurich, Zurich 8091, Switzerland
[3]Department of Computer Science, ETH Zurich, Zurich 8092, Switzerland
[4]University Children's Hospital Basel, Basel 4056, Switzerland
[5]Department of Biomedical Engineering, University of Basel, Allschwil 4123, Switzerland
[6]Institute of Pharmacology and Toxicology, University of Zurich, Zurich 8057, Switzerland
[7]Lead contact
*Correspondence: steven.brown@pharma.uzh.ch (S.A.B.), malcolm.kohler@usz.ch (M.K.)
https://doi.org/10.1016/j.celrep.2021.109903

SUMMARY

Sleep is crucial to restore body functions and metabolism across nearly all tissues and cells, and sleep restriction is linked to various metabolic dysfunctions in humans. Using exhaled breath analysis by secondary electrospray ionization high-resolution mass spectrometry, we measured the human exhaled metabolome at 10-s resolution across a night of sleep in combination with conventional polysomnography. Our subsequent analysis of almost 2,000 metabolite features demonstrates rapid, reversible control of major metabolic pathways by the individual vigilance states. Within this framework, whereas a switch to wake reduces fatty acid oxidation, a switch to slow-wave sleep increases it, and the transition to rapid eye movement sleep results in elevation of tricarboxylic acid (TCA) cycle intermediates. Thus, in addition to daily regulation of metabolism, there exists a surprising and complex underlying orchestration across sleep and wake. Both likely play an important role in optimizing metabolic circuits for human performance and health.

INTRODUCTION

At the most basic level, humans spend daytime awake, moving and feeding, and nighttime asleep, quiescent and fasting. Considerable research has established that metabolism across the brain and body is regulated in a daily "circadian" fashion, complementing this pattern. Even in the absence of daily cues, most aspects of this metabolic control persist, directed by an endogenous molecular clockwork (Reinke and Asher, 2019). However, systematic disruption of circadian patterns of activity, for example by shiftwork, results in considerable disruptions to normal metabolic patterns, and such disruption is believed to underlie the linkage between shiftwork and metabolic syndrome (a spectrum of disorders, including obesity, diabetes, and cardiovascular morbidity, that are associated with metabolic dysfunction) (Kervezee et al., 2020).

Overlaying this daily pattern is the sleep-wake cycle itself, a complex repetitive cycle of distinct brain states. Mammalian sleep is divided into rapid eye movement (REM) sleep and non-REM (NREM) sleep based on electroencephalogram (EEG) and electromyogram (EMG) measurements. In humans, within NREM sleep, three different stages are further differentiated; N1 and N2 sleep are considered as gradual changes from wakefulness toward slow-wave sleep (SWS) or deep sleep (N3) (Kales and Rechtschaffen, 1968). Sleep amount is driven both by circadian influences and by a separate homeostatic process, with increasing time awake favoring increased sleep (Borbély et al., 2016). Independently of circadian disruptions, impaired sleep is also associated with major physiological and psychological sequelae, such as impaired glucose and lipid metabolism, cardiovascular disease, and impaired psychological and social functioning, with enormous socioeconomic consequences (Kecklund and Axelsson, 2016). Common sleep disorders are themselves often associated with metabolic syndrome. For example, obstructive sleep apnea (OSA) is linked to dyslipidemia, glucose intolerance, and type 2 diabetes, while different forms of insomnia are correlated with impaired glycemic control (Briançon-Marjollet et al., 2015).

Much of our knowledge of the control of metabolism by circadian clocks and sleep in humans comes from metabolomics, the systematic study of small molecules produced by anabolic and catabolic reactions, which can be sampled periodically across the day from blood, urine, and saliva (Ang et al., 2012; Dallmann et al., 2012; Bell et al., 2013; Davies et al., 2014; Skene et al., 2018; Grant et al., 2019; Kervezee et al., 2019; Honma et al., 2020; Hancox et al., 2021). These have been complemented by sampling accessible tissues, such as blood and adipose tissue, across time and analyzing the temporal pattern of RNAs (transcriptomics) or proteins (proteomics) therein (Spörl et al., 2012; Robles and Mann, 2013; Archer et al., 2014; Christou et al., 2019). From these studies, up to 20% of all metabolites vary with time of day, and this oscillation can be disrupted by

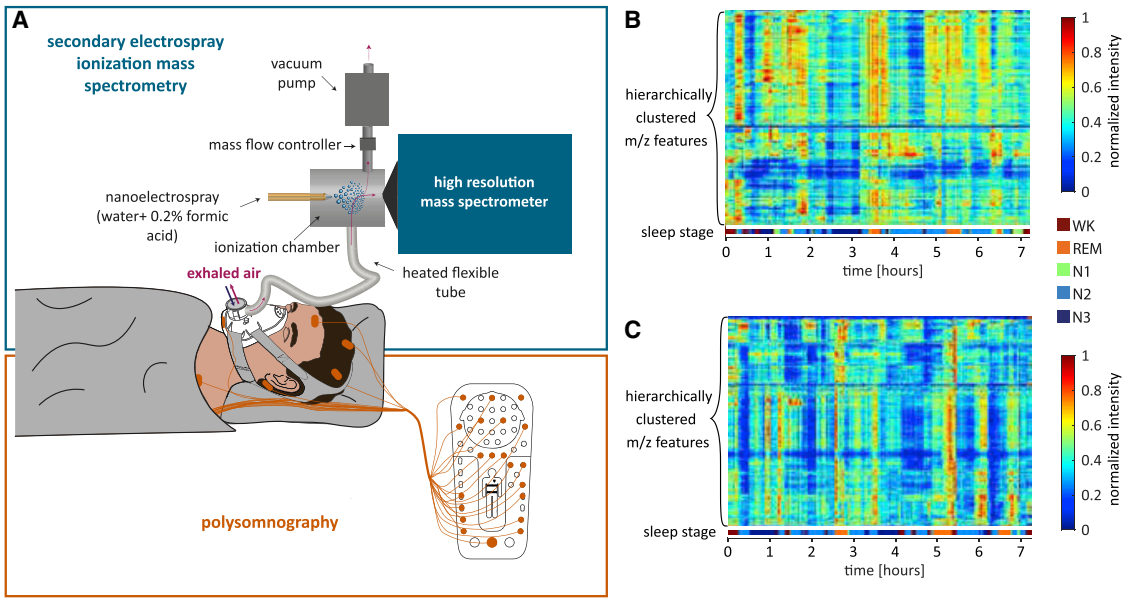

Figure 1. Real-time breath analysis during sleep by SESI-HRMS

(A) Experimental setup. Exhaled breath was sampled continuously with a mask, which was connected directly to the ionization source via a heated flexible tube. Molecules were ionized in the electrospray consisting of water and formic acid. Sample flow was controlled at the exhaust of the SESI source. Ions were detected with a high-resolution time-of-flight mass spectrometer. In parallel, a full polysomnography was performed.

(B and C) Heat maps of 1,271 m/z features detected in positive ionization mode (B) and 725 m/z features detected in negative ionization mode (C) over time in one subject after feature-wise baseline subtraction. Sleep stages are labeled on the bottom of the heat maps and scale bars represent normalized intensity.

circadian misphasing (shiftwork) (Kervezee et al., 2019) and by sleep restriction (Bell et al., 2013) or sleep deprivation (Davies et al., 2014). The following multiple overarching and logical themes emerge: carbon energy storage as glycogen during wake/daytime and its breakdown during sleep/nighttime and energy expenditure-related pathways during wake, followed by synthesis and regeneration during sleep (Petit et al., 2015).

Although global metabolic rate (for example, oxygen consumption and CO_2 production as a measure of differences in energy expenditure and glucose utilization) has been measured across sleep (Brebbia and Altshuler, 1965; Fontvieille et al., 1994; Kayaba et al., 2017), changes in metabolic regulation on a molecular level across different sleep stages remain unexplored. This is mainly due to a lack of sufficient sampling rates for biofluids or tissues. Taking advantage of secondary electrospray ionization coupled to a high-resolution mass spectrometer (SESI-HRMS) (Gaugg et al., 2016), our groups have overcome these difficulties by analyzing exhaled breath. Breath analysis provides real-time information within seconds in a non-invasive fashion. Hundreds of metabolites have been reported from breath, including fatty acids, amino acids, and tricarboxylic acid (TCA) cycle intermediates (de Lacy Costello et al., 2014; Bruderer et al., 2019). We have pioneered the use of these technologies for circadian measurements across the day (Sinues et al., 2013; Martinez-Lozano Sinues et al., 2014) and for identification of molecular alterations present in various diseases during daytime (Schwarz et al., 2016; Bregy et al., 2018; Gaisl et al., 2018; Gaugg et al., 2019). Here, by delivering breath to our SESI-HRMS across a night of sleep while simultaneously conducting polysomnography, we provide a glimpse of the human exhaled metabolome at unprecedented 10-s resolution across sleep stages during a full night of sleep.

RESULTS

Breath analysis during sleep

We analyzed exhaled breath of healthy individuals while they were sleeping in order to access metabolic pathway activity during different states of vigilance (see workflow, Figure 1A; Figure S1). Making use of the non-invasive and very high sampling frequency of SESI-HRMS breath analysis, we were able to access the human metabolome with an average depth of about 2,000 metabolite features per time point during sleep with a time resolution of 10 s while performing polysomnography in parallel (Figure 1A). In total, 13 healthy individuals with a normal sleep architecture (Table S1) were analyzed, and we were able to detect over time the traces of 1,996 metabolite features with distinct mass-to-charge ratios (m/z). These traces were baseline subtracted in order to remove confounding gradual changes in metabolite time profiles across the night and then correlated with individual sleep stages (see sample heat maps in Figures 1B and 1C; heat maps for all individuals are given in Figures S2 and S3; Data S1). In each individual, clear indications of families of sleep-regulated metabolites were visible as vertical stripes in these heat maps.

Sleep stage-specific metabolic patterns

In order to access whether there is noteworthy differential metabolic regulation globally across different stages of sleep, we first visualized median mass spectra of each sleep stage of all study

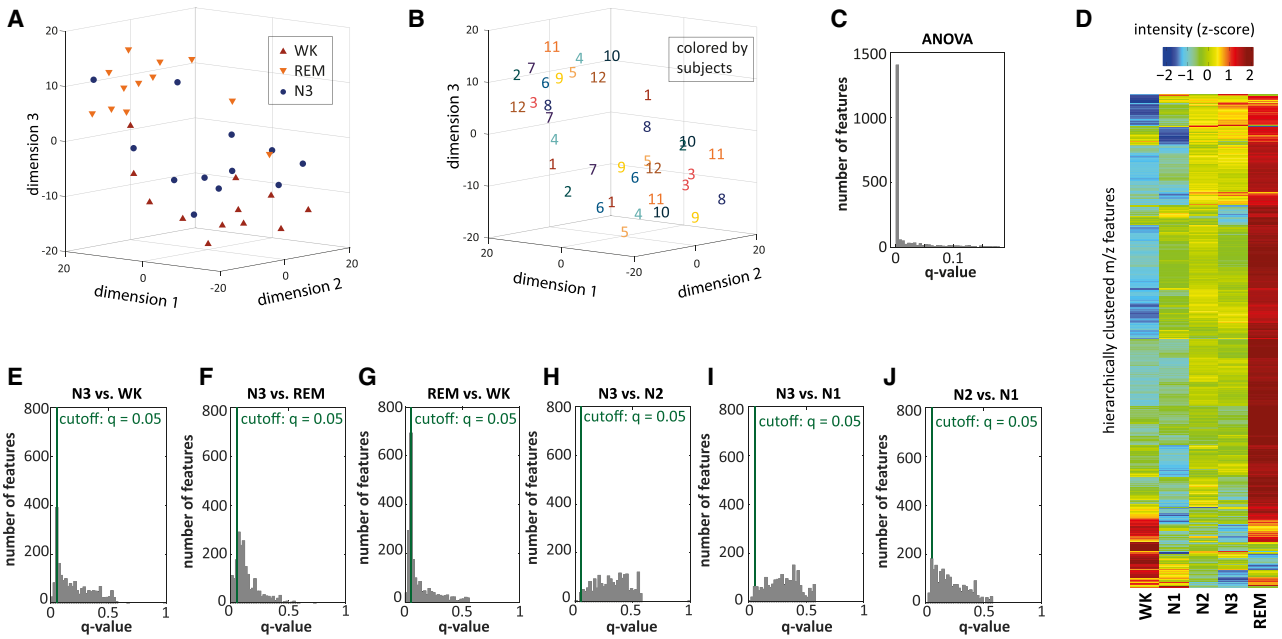

Figure 2. Metabolic fingerprints of different sleep stages

(A and B) Visualization of median breath spectra during N3 sleep, REM sleep, and wakefulness after dimension reduction by t-distributed stochastic neighbor embedding. Data points are colored by sleep stage (A) or colored and numbered subjects, respectively (B); n = 12.

(C) Q value distribution of analysis of variance testing for differences between a model accounting for different effects of sleep stages and a model not accounting for these differences (n = 12). For 1,277 features, we obtained q values below 0.001. This indicates sleep stage-specific regulation of a major part of the metabolome.

(D) Heat map representing the median intensity (*Z* scored) of each sleep stage for these 1,277 features clustered hierarchically (n = 12).

(E–J) Q value distributions from pairwise comparisons of N3 vs. wake (E), N3 vs. REM (F), REM vs. wake (G), N3 vs. N2 (H), N3 vs. N1 (I), N2 vs. N1 (J). While comparisons of N3 sleep, REM sleep, and wakefulness revealed metabolic differences between these states, flat q value distributions obtained from comparisons between N1, N2, and N3 suggest similarity between those stages also on a metabolic level (n= 12).

subjects after dimension reduction. We found that spectral data of different people belonging to the same stage of vigilance cluster together (Figure 2A), whereas we did not observe clustering of different vigilance states according to subjects (Figure 2B). Thus, relative metabolite levels observed in different vigilance states are similar across different subjects, while different vigilance states in the same subject are not similar. Using analysis of variance individually for each metabolite, we then tested how a model considering sleep states to affect metabolite levels in breath performs compared with the null hypothesis of a model that does not consider sleep stages and generated q value distributions of all metabolites. Remarkably, for most of the detected m/z features (1,277 features), a significant association with vigilance state ($q < 0.001$) is observed (Figure 2C). Adding support to this hypothesis, numerous significant differences are seen between all major sleep-wake states (NREM, REM, and wake [Figures 2D–2G]). By contrast, far fewer differences were observed among metabolites across related sleep states (N1-, N2-, and N3-NREM sleep; Figures 2D and 2H–2J). Therefore, we did not consider N1 and N2 sleep in our further analysis.

Immediate metabolic regulation

To further investigate the nature of these sleep state-dependent metabolic patterns, we followed two approaches of analysis. First, we performed pairwise comparisons of breath metabolite levels during different sleep stages using Wilcoxon signed rank tests in order to detect rapid changes in levels of individual metabolites. An example of a single metabolite from a few hours of sleep in three individuals is shown in Figure 3A, and a box plot of this metabolite across all subjects and sleep stages is shown in Figure 3B. Numerical comparisons across all subjects and features are summarized in Figure 3C, with individual metabolites from this Venn diagram listed in Table S3A. Sample box plots coming from comparisons across all subjects and different sleep stages are shown in Figure 3D (we present box plots for all identified metabolites further below). We found significant differences ($q < 0.05$) between REM sleep and wakefulness for 842 m/z features. Relative concentrations of 411 features differed between N3 sleep and wakefulness, and 312 features had different levels during REM sleep and N3 sleep (Figure 3C) (numbers of significantly different features at other q value cutoffs can be seen in Figure S4).

In order to move beyond the discovery of simple pairwise correlations of time series variables (in our case, a particular metabolite and a particular sleep stage) toward identifying directed ("causal") interactions that could characterize functional circuits relating sleep and metabolism, we next developed a neural network-based method to infer Granger causal relationships. The concept of Granger causality was previously very successfully applied in the domains of economics (Granger, 1969) and

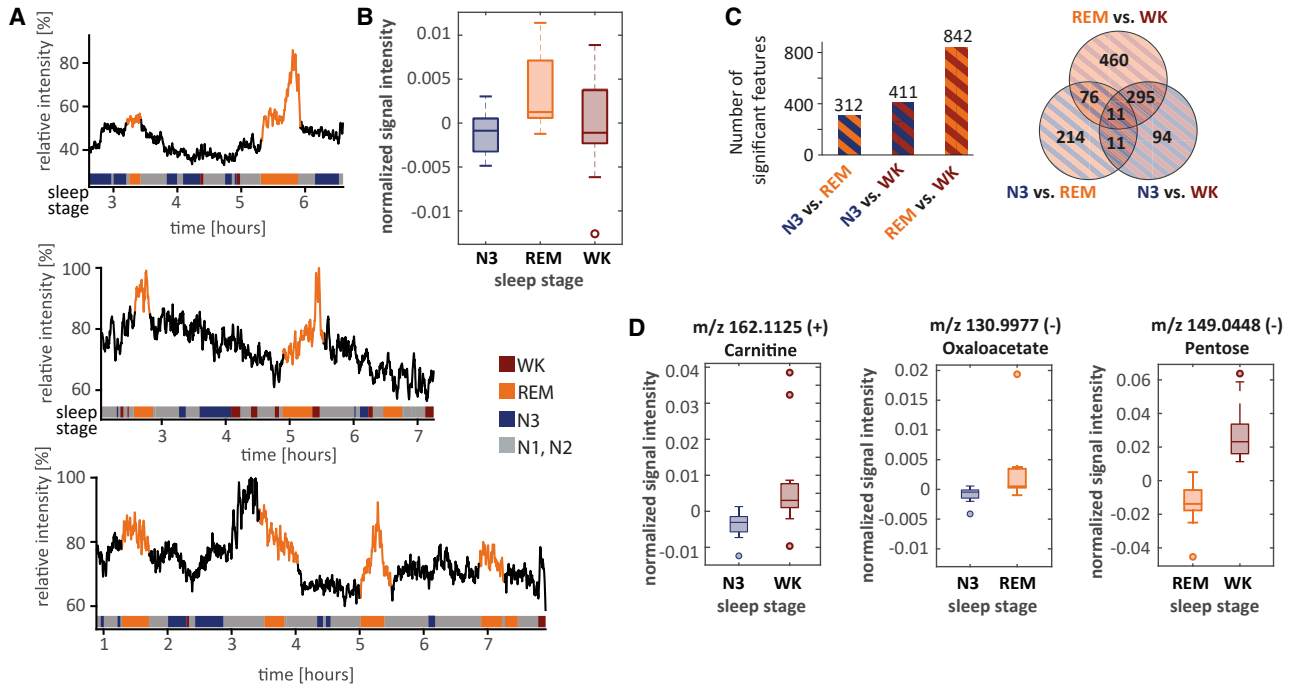

Figure 3. Pairwise comparisons unravel instantaneous metabolic response to sleep stage transitions

(A) Time traces of m/z 149.0237 (negative mode, hereafter abbreviated as "−") in three individuals, showing the direct increase of metabolite levels with REM sleep. We detected such metabolites using conventional comparative statistics.

(B) Resulting box plot (center line: median; box limits: 25th and 75th percent quantile; whisker length: 1.5 interquartile range; n = 12) of metabolite shown in (A).

(C) Pairwise comparisons of mean breath spectra in Wilcoxon signed ranked tests suggest significant differential regulation of hundreds of metabolites across different stages of sleep as presented in the bar plot (n = 13). The Venn diagram shows that there are overlaps between the sets of significant m/z features.

(D) Box plots (center line: median; box limits: 25th and 75th percent quantile; whisker length: 1.5 interquartile range) of three metabolites identified as carnitine (n = 13), oxaloacetate (n = 13), and pentose (n = 13) showing significantly different levels in breath during N3 sleep and wakefulness, during N3 and REM sleep, and during REM sleep and wakefulness, respectively. In addition, a time trace and box plot are provided for isoprene in Data S1.

neuroscience (Seth et al., 2015). Our Granger causality framework (fully described in the supplementary information) offers an alternative view of our data based upon the concept of predictability, the idea that the most significant sleep-related metabolites can be used to predict sleep states. Importantly, this framework also detects non-linear and time-delayed relationships, which are common in multistep metabolic pathways. Potential advantages of this computational approach are extensively discussed in the supplementary information. Our analysis based on Granger causality resulted in 386, 196, and 135 features associated with wakefulness, REM sleep, and N3 sleep, respectively, many of which (182, 60, and 59) were not identified by our initial conventional approach. An example of a metabolite identified with this approach is shown in Figure 4A for a few hours of sleep in three individuals. Numerical comparisons across all subjects and features are summarized in Figure 4B, with individual features listed in Table S3A.

Pathway mapping of mass spectrometry features: Sleep stages control axes of metabolism

To understand the cellular physiology underlying the metabolic regulation triggered by sleep stages, we next performed compound identification and pathway analysis. Compound identification is still the biggest challenge in the field of metabolomics. Nevertheless, more and more tools are being developed for automated compound annotation (Chaleckis et al., 2019). We used an annotation algorithm that combines information about elemental composition obtained from the accurately measured mass with metabolic pathway mapping and enrichment analysis (Li et al., 2013). In this way, possible errors in the identification of any individual compound are "averaged out" against the expectation that quantitative differences would be observed across multiple metabolites within a given pathway. Because automated annotation is still prone to false positives, we investigated top pathway hits further manually and confirmed the identities of several compounds with tandem mass spectrometry data from liquid chromatography-mass spectrometry measurements of exhaled breath condensate or from real-time breath measurements (Figure S5).

Considering the full set of annotated compounds whose abundance varies with vigilance state, we found that the activity of most major axes of cellular metabolism, such as lipid metabolism, carbohydrate metabolism, and TCA cycle activity, are in fact strongly sleep-wake state dependent (Figure 5; box plots of all compounds are in Figure S6 and quantitative results are in Table S3B).

For example, we were able to identify short-chain acylcarnitines (ACs) in exhaled breath (Figures 6A–6C; Figures S7A and

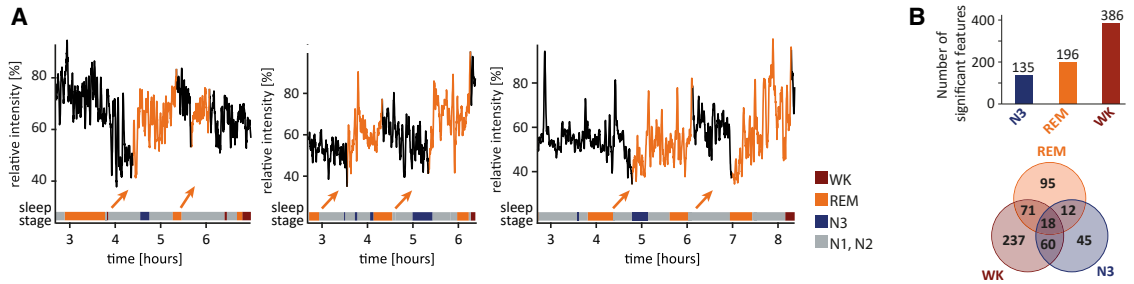

Figure 4. Inferring non-linear Granger causality with neural networks reveals more complex patterns

(A) Time traces of m/z 181.06 (−) in three individuals. Metabolite levels were rising slowly after the occurrence of REM sleep. Our analysis based on Granger causality unraveled such more complex temporal relationships.

(B) Results from inferring non-linear Granger causality with neural networks suggest causal relationships between several hundreds of m/z features and N3 sleep, REM sleep, and wakefulness as shown in the bar plot (n = 13). The Venn diagram shows that these sets of features are overlapping.

S7B), and we found breath levels of short-chain ACs to be highest during wakefulness and lowest during N3 sleep (Figure 6D). For most of them, we additionally found Granger causal relationships to wakefulness and/or N3 sleep. We did not detect significant differences in carnitine levels between N3 and REM sleep. Thus, systemic changes in fatty acid oxidation are occurring across sleep and wake (yellow quadrant, Figure 5): a switch to wake increases fatty acid oxidation, whereas a switch to NREM sleep reduces it.

Similarly, we found several metabolites involved in propanoate and butanoate metabolism to be downregulated during NREM sleep, and for propanoate and aminobutanoate, we also found Granger causal indications of this connection (green quadrant, Figure 5). These molecules are natural byproducts of fat and protein metabolism.

We observed increased levels of several TCA cycle intermediates during REM sleep (brown quadrant, Figure 5). We also found malate and oxaloacetate to be Granger causally related with REM sleep (succinate was not upregulated during REM sleep). Because normally REM sleep can only follow NREM sleep, a transition to REM sleep results in elevation of TCA cycle intermediates, possibly preparing for mitochondrial oxidation later in wake.

Finally, when examining glycolysis, we found highest glucose levels in breath during wakefulness and lowest levels during REM sleep. We observed a similar behavior for several other metabolites involved in the pentose phosphate pathway and in pentose and glucoronate interconversions. For most of them, we also found Granger causal relationships with REM sleep and wakefulness. By contrast, we found opposite trends for pyruvate levels, which were increased during REM sleep and lowest during wakefulness. In addition, for many metabolites involved in carbohydrate metabolism, we observed significant differences between REM sleep and N3 sleep (purple and turquoise quadrants, Figure 5).

DISCUSSION

By taking advantage of metabolites present in human breath, our studies measure the human metabolome non-invasively at the unprecedented resolution of 10 s across the night. Such exhaled metabolites are mainly the product of diffusion across the lung alveolar membrane and therefore are thought to resemble the composition of the blood metabolome with additional contributions from the upper airways (Ross and Babgi, 2017). We have separately verified this in nine subjects, comparing the results of the metabolome in blood draws during wakefulness to those obtained from breath at the same time point. Levels of ACs correlate well with blood levels (Figures S7C–S7E), indicating that breath levels are reflecting systemic carnitine levels. We also verified this relation between breath and blood metabolites for representatives of other metabolic pathways, such as the TCA cycle (fumarate), glycolysis (lactate), propionate metabolism (lactate), and the pentose phosphate pathway (glycerate) (Figure S7F).

Our results imply that a major part of the human metabolome is subjected to sleep stage-specific regulation. As mentioned above, this question has been hitherto difficult to address due to issues of sampling rate versus sleep stage duration. However, our studies are in agreement with existing data of which we are aware. For example, isoprene has been studied previously with respect to leg movements during sleep and muscle atonia during REM sleep (King et al., 2012). Among the detected molecules, we identified isoprene and observed decreased isoprene levels during REM sleep and spikes in exhaled isoprene associated with leg movements (Data S1).

In our study, we found extensive and immediate metabolic responses unique to REM sleep, N3 sleep, and wakefulness as well as metabolites with a more complicated but predictable temporal relationship to vigilance states. Metabolic patterns of N1, N2, and N3 sleep did not differ significantly across adjacent stages, indicating that the gradual transition from wakefulness to deep sleep across these three states is reflected as well on a metabolic level.

Mechanistically, our data could be interpreted in two directions: sleep stage changes driving metabolism or metabolism driving sleep stage changes. While we favor the former, only subsequent elucidation of specific control mechanisms will fully clarify this question.

Free carnitine is rate limiting for the transport of long-chain fatty acids across the mitochondrial membrane to be oxidized (Longo et al., 2016), and supplementation with L-carnitine is

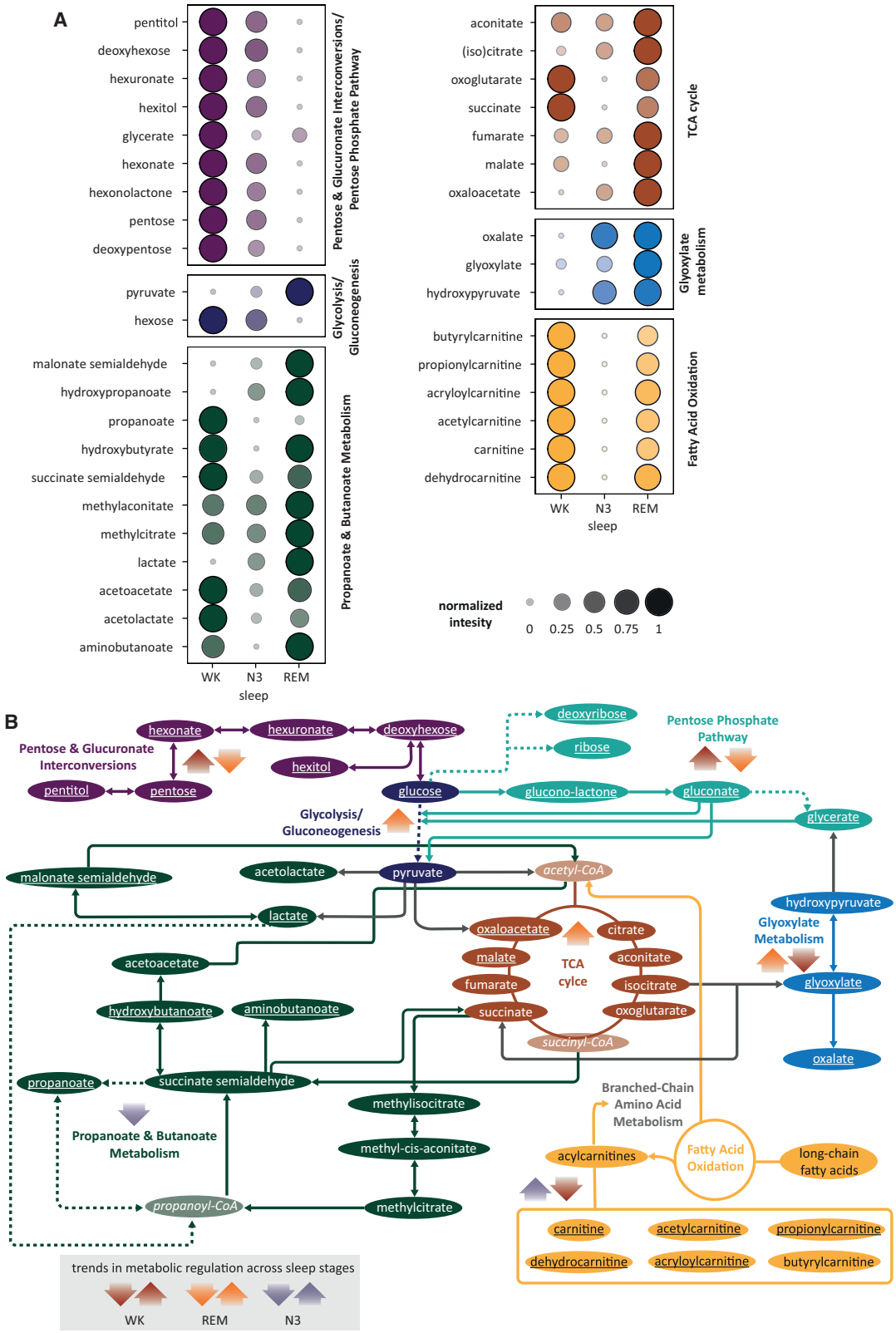

(legend on next page)

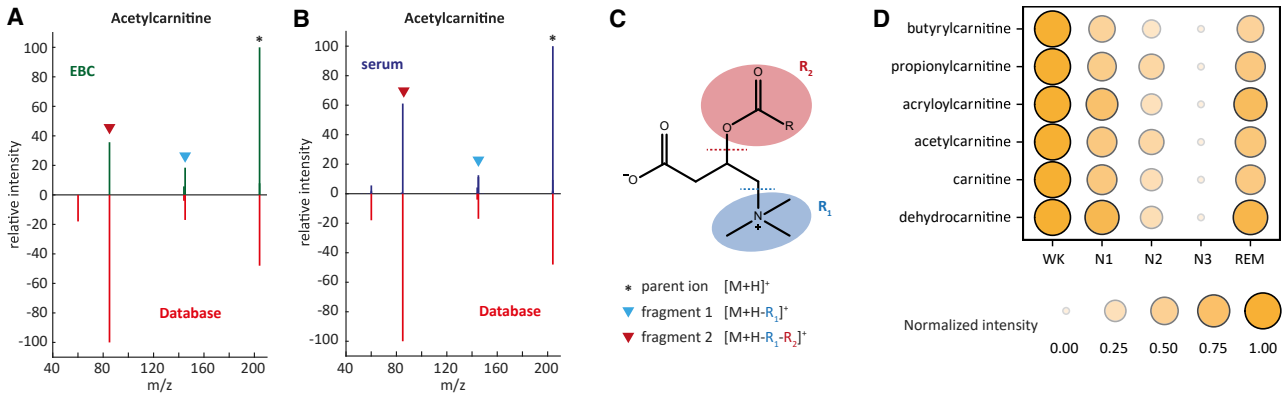

Figure 6. Acylcarnitines in breath during sleep.

(A and B) Unprecedented identification of acylcarnitines in exhaled breath. Tandem mass spectrometry (MS-MS) spectra of acetylcarnitine obtained from exhaled breath condensate (A) and serum (B) in comparison with database MS-MS spectra.

(C) Fragmentation pattern of acylcarnitines reported in the literature (Giesbertz et al., 2015).

(D) Median intensities of short-chain acylcarnitines in breath during the different sleep stages (n = 12). The intensities were scaled between 0 and 1 for each compound. Carnitine levels are decreasing continuously from wakefulness to N3 sleep.

even able to increase fatty acid oxidation directly (Rodgers et al., 2020). ACs of different lengths are intermediary products of this oxidation process. When β-oxidation of fatty acids is impaired or incomplete, this can lead to accumulation of ACs of different lengths. Such accumulation has been observed in patients suffering from metabolic diseases (Adams et al., 2009; Zhao et al., 2020). While long-chain ACs originate predominately from lipid metabolism, short-chain ACs, especially propionylcarnitine, can also be derived from branched-chain amino acid catabolism (McCann et al., 2021).

In this study, we found a decrease of free carnitine as well as short-chain AC levels during N3 sleep compared with wakefulness as well as a gradual decrease in carnitine and AC levels from wake over N1, N2, and N3 NREM sleep (Figure 6). Our findings are in agreement with Davies et al. (2014), who reported increased long-chain AC levels during sleep deprivation compared with sleep. These results suggest that ACs are utilized during N3 sleep and that energy consumption by fatty acid degradation is favored during sleep. This is consistent with respiratory quotient measurement and metabolic labeling studies demonstrating greater relative reliance on fatty acid β-oxidation during the sleep (fasting) phase of the diurnal cycle (Aalling et al., 2018). Our lack of observed differences in valine and (iso)leucine levels between wakefulness and SWS may indicate that the changes in short-chain AC levels do not result from alterations of branched-chain amino acid breakdown. However, we cannot ascertain that they reflect only fatty acid oxidation because we cannot detect long-chain AC from breath. Free carnitine may even play a direct role in the sleep-wake process; administration of L-carnitine was found to decrease daytime sleepiness in narcolepsy patients (Miyagawa et al., 2013).

From our results for pathways involved in carbohydrate metabolism, we hypothesize increased glucose utilization via glycolysis during REM sleep. This assumption is in line with the previously reported decrease in glucose utilization during NREM sleep compared with REM sleep (Van Cauter et al., 1997). Increased pyruvate production via glycolysis during REM sleep goes along with increased TCA cycle activity during REM sleep induced by increased feeding from pyruvate via oxaloacetate, as suggested by our findings on TCA cycle intermediates.

Furthermore, there is evidence that the TCA cycle is involved in immune reprogramming (Galván-Peña and O'Neill, 2014). Macrophage activation and cytokine production can be triggered by checkpoints in the TCA cycle, most notably after citrate/isocitrate and after succinate, increasing these intermediates (Williams and O'Neill, 2018). In addition, sleep is associated with anti-inflammatory function (Gómez-González et al., 2012). Our failure to see upregulated succinate during REM sleep in combination with our finding of upregulation of its successors fumarate and malate might indicate that this checkpoint is not activated, making REM sleep anti-inflammatory.

Sleep loss has been associated with impaired glucose metabolism (Knutson, 2007). Recently, circulating propanoate levels have been associated positively with insulin sensitivity (Müller et al., 2019). Based on these discoveries, one may hypothesize from our findings of downregulated propanoate and butanoate

Figure 5. Metabolic pathways with differential regulation across different stages of vigilance

(A) Median intensities during N3 sleep, REM sleep, and wakefulness are represented for identified metabolites of major pathways by size and opacity (scaled from 0 to 1 feature wise). Colors represent the different pathways; n = 12 for metabolites detected in negative mode, and n = 13 for metabolites detected in positive mode.

(B) Metabolic pathway map showing these compounds with sleep state-dependent regulation. Metabolites in italic font in transparent ovals are not detected. Solid ovals indicate metabolites showing significant differences. Underlined compounds additionally exhibit a Granger causal relationship between metabolite level and at least one sleep stage. Metabolic up- or downregulation during sleep stages is indicated for each pathway with arrows. Dashed lines indicate omitted molecules. Corresponding box plots of all indicated compounds are provided in Figure S6, and numeric results are in Table S3B.

Table 1. Participant characteristics	
Age (mean ± SD, years)	29.2 ± 8.3
Sex (male participants, %)	57
Body mass index (mean ± SD, kg/m^2)	22 ± 3
Smoking state	
Active smokers (%)	7
Ex-smokers (%)	7

SD, standard deviation.

metabolism during N3 sleep that short-chain fatty acids act as mediators for decreased insulin sensitivity during SWS.

In recent years, circadian regulation of metabolism has received enormous attention, and many aspects of cellular metabolism are also under circadian control, often in a tissue-specific fashion. (Li et al., 2012). Sleep timing is a major output of circadian clock function, and disruption of both clocks and sleep is associated with metabolic diseases (Knutson and Van Cauter, 2008; Kelly et al., 2018). Therefore, how circadian control of metabolism overlaps with the vigilance state-dependent metabolism we document remains an important question. In this study, we did not control for circadian rhythms or measure circadian phase, but metabolic regulation by the circadian clock has been studied previously by our lab and others, including by metabolomics and exhalomics (Dallmann et al., 2012; Martinez-Lozano Sinues et al., 2014; Dyar et al., 2018; Cedernaes et al., 2019; Kervezee et al., 2019). Despite different sample types and different analysis techniques, we detected 247 of the m/z features reported in these circadian studies also in our study of exhaled breath during sleep (Data S2). Among these commonly detected metabolites, the major part (42.5%) is regulated by both sleep stages and circadian clocks; 16.2% are controlled by circadian clocks only, and 28.3% are only associated with sleep states. This comparison of our sleep state-dependent data and the results from previous circadian studies suggests that circadian and sleep-dependent regulation of metabolism may represent an interlocked network of metabolic control analogous to the overlapping layers of control that we have described recently for the sleep- and circadian-dependent transcriptome (Noya et al., 2019).

Limitations of the study

Although our dataset identifies over 1,000 sleep state-regulated m/z features, the pathways subject to sleep-dependent regulation found in this study are probably only scratching the surface of such metabolic regulation. Further studies will improve the identification of unknown compounds and thus enlarge pathway coverage. Moreover, it might be interesting to further investigate kinetic effects in future studies. Using two different statistical frameworks, our study has found extensive correlation between metabolite levels and sleep stages. In particular, for the second of these frameworks (Granger causality), our correlations disregard any time bias. Thus, we are able to find correlations across the entirety of a sequential biochemical pathway rather than only in its proximal step. For many metabolites, our results from Granger causality show a time lag between sleep-stage switch and metabolic alterations for a number of metabolites. From visual inspection of the corresponding time traces, we conclude that the timing is different for different metabolites. This would be expected because sleep-controlled metabolic pathways would have individual steps with different phase relationships to sleep state transitions. However, our algorithm distinguishes only between metabolites with and without a relationship to sleep stages, and we cannot retrieve any quantitative information about the temporal pattern, such as lag time. It would be interesting to implement this in future studies, potentially showing which biochemical steps are directly regulated by sleep stage and which are indirect consequences of upstream or downstream sleep-regulated events. In addition, one could study if the length of a sleep state plays a role. Because we binned data for each sleep stage, we cannot make any statement about the influence of sleep stage length on metabolite levels detected. However, this might become an interesting subject of future studies; with reproducible quantifications across individuals, it might then be possible to determine previous amounts of wake or of a particular sleep state. This would be a useful metric for the diagnosis of sleep disorders or even of adequate sleep in general.

Further, one must be aware of the limited explanatory power of Granger causality analysis for not ''causally sufficient'' variables (Peters et al., 2017). For example, if ''superior'' mechanisms exist that regulate both metabolism and sleep, statements of causality between ion intensities and sleep phases could be meaningless. Therefore, future mechanistic studies are required to validate our findings.

In conclusion, by analyzing exhaled breath during sleep, we found unprecedented indications for sleep states as organizers of cellular metabolism. Not only circadian patterns but also sleep-wake patterns dynamically seem to program metabolism, providing precise timing for carbohydrate synthesis and degradation, fatty acid oxidation, and the mitochondrial TCA cycle. Thereby, they might directly connect sleep patterns to metabolic homeostasis and health.

STAR★METHODS

Detailed methods are provided in the online version of this paper and include the following:

- KEY RESOURCES TABLE
- RESOURCE AVAILABILITY
  - Lead contact
  - Materials availability
  - Data and code availability
- EXPERIMENTAL MODEL AND SUBJECT DETAILS
  - Sleep experiment
  - Blood-breath comparison experiments
- METHOD DETAILS
  - SESI-HRMS measurements during sleep
  - Polysomnography
  - Blood breath comparison experiments
  - UPLC-tandem-MS measurements of serum
- QUANTIFICATION AND STATISTICAL ANALYSIS
  - Data preprocessing
  - Statistics
  - One-way ANOVA
  - Pairwise comparisons

- Inferring non-linear Granger causality with neural networks
- Granger causality
- Limitations of Granger causality
- Model
- Bootstrapping
- Time reversal
- Hyperparameters and network specification
- Cross-validation
- Simulation experiments
- Pathway enrichment analysis and compound ID
- Blood-breath comparison experiments

SUPPLEMENTAL INFORMATION

Supplemental information can be found online at https://doi.org/10.1016/j.celrep.2021.109903.

ACKNOWLEDGMENTS

We acknowledge Luzia Gyr, Bettina Streckenbach, Martin Gaugg, Tobias Bruderer, and Jiayi Lan for scientific discussion. This project is part of the Zurich Exhalomics project, a flagship project of "University Medicine Zurich." Further funding was obtained from the Velux Foundation (project number 1072 to P.S. and S.A.B.). P.S. gratefully acknowledges the Fondation Botnar for sponsoring his professorship.

AUTHOR CONTRIBUTIONS

M.K., S.A.B., P.S., R.Z., N.N., and T.G. designed the study. T.G., M.K., and P.S. wrote the ethics protocol. N.N., T.G., and M.O. performed the experiments. N.N. analyzed all mass spectrometry data and performed statistical analysis. T.G. analyzed the polysomnography data. D.M., R.M., S.B., and J.B. developed the algorithm based on Granger causality. M.K., S.A.B., P.S., N.N., T.G., and R.Z. contributed to the discussion and interpretation of the results. N.N., R.M., S.A.B., and M.K. wrote the manuscript with input from the other co-authors.

DECLARATION OF INTERESTS

M.K. and P.S. are co-founders of a company employing SESI-MS commercially, Deep Breath Intelligence (DBI).

Received: March 30, 2021
Revised: September 14, 2021
Accepted: October 6, 2021
Published: October 26, 2021

SUPPORTING CITATIONS

The following references appear in the Supplemental information: Brooks and Peever (2008); King et al. (2010); Redline et al. (2004); Tejero Rioseras et al. (2018).

REFERENCES

Aalling, N.N., Nedergaard, M., and DiNuzzo, M. (2018). Cerebral Metabolic Changes During Sleep. Curr. Neurol. Neurosci. Rep. *18*, 57. https://doi.org/10.1007/s11910-018-0868-9.

Adams, S.H., Hoppel, C.L., Lok, K.H., Zhao, L., Wong, S.W., Minkler, P.E., Hwang, D.H., Newman, J.W., and Garvey, W.T. (2009). Plasma acylcarnitine profiles suggest incomplete long-chain fatty acid β-oxidation and altered tricarboxylic acid cycle activity in type 2 diabetic African-American women. J. Nutr. *139*, 1073–1081. https://doi.org/10.3945/jn.108.103754.

Ang, J.E., Revell, V., Mann, A., Mäntele, S., Otway, D.T., Johnston, J.D., Thumser, A.E., Skene, D.J., and Raynaud, F. (2012). Identification of human plasma metabolites exhibiting time-of-day variation using an untargeted liquid chromatography-mass spectrometry metabolomic approach. Chronobiol. Int. *29*, 868–881. https://doi.org/10.3109/07420528.2012.699122.

Archer, S.N., Laing, E.E., Möller-Levet, C.S., van der Veen, D.R., Bucca, G., Lazar, A.S., Santhi, N., Slak, A., Kabiljo, R., von Schantz, M., et al. (2014). Mistimed sleep disrupts circadian regulation of the human transcriptome. Proc. Natl. Acad. Sci. USA *111*, E682–E691. https://doi.org/10.1073/pnas.1316335111.

Bell, L.N., Kilkus, J.M., Booth, J.N., III, Bromley, L.E., Imperial, J.G., and Penev, P.D. (2013). Effects of sleep restriction on the human plasma metabolome. Physiol. Behav. *122*, 25–31. https://doi.org/10.1016/j.physbeh.2013.08.007.

Borbély, A.A., Daan, S., Wirz-Justice, A., and Deboer, T. (2016). The two-process model of sleep regulation: A reappraisal. J. Sleep Res. *25*, 131–143. https://doi.org/10.1111/jsr.12371.

Brebbia, D.R., and Altshuler, K.Z. (1965). Oxygen consumption rate and electroencephalographic stage of sleep. Science *150*, 1621–1623. https://doi.org/10.1126/science.150.3703.1621.

Bregy, L., Nussbaumer-Ochsner, Y., Martinez-Lozano Sinues, P., García-Gómez, D., Suter, Y., Gaisl, T., Stebler, N., Gaugg, M.T., Kohler, M., and Zonobi, R. (2018). Real-time mass spectrometric identification of metabolites characteristic of chronic obstructive pulmonary disease in exhaled breath. Clin. Mass. Spectrom. *7*, 29–35. https://doi.org/10.1016/j.clinms.2018.02.003.

Briançon-Marjollet, A., Weiszenstein, M., Henri, M., Thomas, A., Godin-Ribuot, D., and Polak, J. (2015). The impact of sleep disorders on glucose metabolism: endocrine and molecular mechanisms. Diabetol. Metab. Syndr. *7*, 25. https://doi.org/10.1186/s13098-015-0018-3.

Brooks, P.L., and Peever, J.H. (2008). Unraveling the mechanisms of REM sleep atonia. Sleep *31*, 1492–1497. https://doi.org/10.1093/sleep/31.11.1492.

Bruderer, T., Gaisl, T., Gaugg, M.T., Nowak, N., Streckenbach, B., Müller, S., Moeller, A., Kohler, M., and Zenobi, R. (2019). On-Line Analysis of Exhaled Breath *Focus Review*. Chem. Rev. *119*, 10803–10828. https://doi.org/10.1021/acs.chemrev.9b00005.

Burton, R.F. (2000). Respiration. Physiology by Numbers: An Encouragement to Quantitative Thinking (Cambridge University Press), pp. 65–91.

Cedernaes, J., Huang, W., Ramsey, K.M., Waldeck, N., Cheng, L., Marcheva, B., Omura, C., Kobayashi, Y., Peek, C.B., Levine, D.C., et al. (2019). Transcriptional Basis for Rhythmic Control of Hunger and Metabolism within the AgRP Neuron. Cell Metab. *29*, 1078–1091.e5. https://doi.org/10.1016/j.cmet.2019.01.023.

Chaleckis, R., Meister, I., Zhang, P., and Wheelock, C.E. (2019). Challenges, progress and promises of metabolite annotation for LC-MS-based metabolomics. Curr. Opin. Biotechnol. *55*, 44–50. https://doi.org/10.1016/j.copbio.2018.07.010.

Chong, J., Wishart, D.S., and Xia, J. (2019). Using MetaboAnalyst 4.0 for Comprehensive and Integrative Metabolomics Data Analysis. Curr. Protoc. Bioinformatics *68*, e86. https://doi.org/10.1002/cpbi.86.

Christou, S., Wehrens, S.M.T., Isherwood, C., Möller-Levet, C.S., Wu, H., Revell, V.L., Bucca, G., Skene, D.J., Laing, E.E., Archer, S.N., et al. (2019). Circadian regulation in human white adipose tissue revealed by transcriptome and metabolic network analysis. Sci. Rep. *9*, 2641. https://doi.org/10.1038/s41598-019-39668-3.

Cohen, J. (1977). Statistical power analysis for the behavioral sciences (Academic Press London).

Dallmann, R., Viola, A.U., Tarokh, L., Cajochen, C., and Brown, S.A. (2012). The human circadian metabolome. Proc. Natl. Acad. Sci. USA *109*, 2625–2629. https://doi.org/10.1073/pnas.1114410109.

Davies, S.K., Ang, J.E., Revell, V.L., Holmes, B., Mann, A., Robertson, F.P., Cui, N., Middleton, B., Ackermann, K., Kayser, M., et al. (2014). Effect of sleep deprivation on the human metabolome. Proc. Natl. Acad. Sci. USA *111*, 10761–10766. https://doi.org/10.1073/pnas.1402663111.

de Lacy Costello, B., Amann, A., Al-Kateb, H., Flynn, C., Filipiak, W., Khalid, T., Osborne, D., and Ratcliffe, N.M. (2014). A review of the volatiles from the healthy human body. J. Breath Res. *8*, 014001. https://doi.org/10.1088/1752-7155/8/1/014001.

Dyar, K.A., Lutter, D., Artati, A., Ceglia, N.J., Liu, Y., Armenta, D., Jastroch, M., Schneider, S., de Mateo, S., Cervantes, M., et al. (2018). Atlas of Circadian Metabolism Reveals System-wide Coordination and Communication between Clocks. Cell *174*, 1571–1585.e11. https://doi.org/10.1016/j.cell.2018.08.042.

Eichler, M. (2012). Causal inference in time series analysis. In Causality - Statistical Perspectives and Applications, C. Berzuini, P. Dawid, and L. Bernardinelli, eds. (Wiley Online Library Chichester), pp. 327–352.

Fontvieille, A.M., Rising, R., Spraul, M., Larson, D.E., and Ravussin, E. (1994). Relationship between sleep stages and metabolic rate in humans. Am. J. Physiol. *267*, E732–E737. https://doi.org/10.1152/ajpendo.1994.267.5.E732.

Fox, J. (2002). Bootstrapping Regression Models. In An R and S-Plus companion to applied regression, J. Fox and G. Monette, eds. (Sage).

Gaisl, T., Bregy, L., Stebler, N., Gaugg, M.T., Bruderer, T., García-Gómez, D., Moeller, A., Singer, F., Schwarz, E.I., Benden, C., et al. (2018). Real-time exhaled breath analysis in patients with cystic fibrosis and controls. J. Breath Res. *12*, 036013. https://doi.org/10.1088/1752-7163/aab7fd.

Galván-Peña, S., and O'Neill, L.A.J. (2014). Metabolic reprograming in macrophage polarization. Front. Immunol. *5*, 420. https://doi.org/10.3389/fimmu.2014.00420.

Gaugg, M.T., Gomez, D.G., Barrios-Collado, C., Vidal-de-Miguel, G., Kohler, M., Zenobi, R., and Martinez-Lozano Sinues, P. (2016). Expanding metabolite coverage of real-time breath analysis by coupling a universal secondary electrospray ionization source and high resolution mass spectrometry–a pilot study on tobacco smokers. J. Breath Res. *10*, 016010. https://doi.org/10.1088/1752-7155/10/1/016010.

Gaugg, M.T., Bruderer, T., Nowak, N., Eiffert, L., Martinez-Lozano Sinues, P., Kohler, M., and Zenobi, R. (2017). Mass-Spectrometric Detection of Omega-Oxidation Products of Aliphatic Fatty Acids in Exhaled Breath. Anal. Chem. *89*, 10329–10334. https://doi.org/10.1021/acs.analchem.7b02092.

Gaugg, M.T., Nussbaumer-Ochsner, Y., Bregy, L., Engler, A., Stebler, N., Gaisl, T., Bruderer, T., Nowak, N., Sinues, P., Zenobi, R., et al. (2019). Real-Time Breath Analysis Reveals Specific Metabolic Signatures of COPD Exacerbations. Chest *156*, 269–276. https://doi.org/10.1016/j.chest.2018.12.023.

Giesbertz, P., Ecker, J., Haag, A., Spanier, B., and Daniel, H. (2015). An LC-MS/MS method to quantify acylcarnitine species including isomeric and odd-numbered forms in plasma and tissues. J. Lipid Res. *56*, 2029–2039. https://doi.org/10.1194/jlr.D061721.

Gómez-González, B., Domínguez-Salazar, E., Hurtado-Alvarado, G., Esqueda-Leon, E., Santana-Miranda, R., Rojas-Zamorano, J.A., and Velázquez-Moctezuma, J. (2012). Role of sleep in the regulation of the immune system and the pituitary hormones. Ann. N Y Acad. Sci. *1261*, 97–106. https://doi.org/10.1111/j.1749-6632.2012.06616.x.

Goodfellow, I., Bengio, Y., and Courville, A. (2016). Deep learning. (MIT press Cambridge).

Granger, C.W.J. (1969). Investigating Causal Relations by Econometric Models and Cross-spectral Methods. Econometrica. *37*, 424–438. https://doi.org/10.2307/1912791.

Grant, L.K., Ftouni, S., Nijagal, B., De Souza, D.P., Tull, D., McConville, M.J., Rajaratnam, S.M.W., Lockley, S.W., and Anderson, C. (2019). Circadian and wake-dependent changes in human plasma polar metabolites during prolonged wakefulness: A preliminary analysis. Sci. Rep. *9*, 4428. https://doi.org/10.1038/s41598-019-40353-8.

Hancox, T.P.M., Skene, D.J., Dallmann, R., and Dunn, W.B. (2021). Tick-Tock Consider the Clock: The Influence of Circadian and External Cycles on Time of Day Variation in the Human Metabolome-A Review. Metabolites *11*, 328. https://doi.org/10.3390/metabo11050328.

Holland, P.W., and Welsch, R.E. (1977). Robust regression using iteratively reweighted least-squares. Commun. Stat. Theory and Methods. *6*, 813–827. https://doi.org/10.1080/03610927708827533.

Honma, A., Revell, V.L., Gunn, P.J., Davies, S.K., Middleton, B., Raynaud, F.I., and Skene, D.J. (2020). Effect of acute total sleep deprivation on plasma melatonin, cortisol and metabolite rhythms in females. Eur. J. Neurosci. *51*, 366–378. https://doi.org/10.1111/ejn.14411.

Iber, C. (2007). The AASM Manual for the Scoring of Sleep and Associated Events: Rules, Terminology and Technical Specifications. (American Academy of Sleep Medicine).

Kales, A., and Rechtschaffen, A. (1968). A manual of standardized terminology, techniques and scoring system for sleep stages of human subjects, National Institutes of Health publication (U.S. National Institute of Neurological Diseases and Blindness, Neurological Information Network).

Kayaba, M., Park, I., Iwayama, K., Seya, Y., Ogata, H., Yajima, K., Satoh, M., and Tokuyama, K. (2017). Energy metabolism differs between sleep stages and begins to increase prior to awakening. Metabolism *69*, 14–23. https://doi.org/10.1016/j.metabol.2016.12.016.

Kecklund, G., and Axelsson, J. (2016). Health consequences of shift work and insufficient sleep. BMJ *355*, i5210. https://doi.org/10.1136/bmj.i5210.

Kelly, R.M., Healy, U., Sreenan, S., McDermott, J.H., and Coogan, A.N. (2018). Clocks in the clinic: circadian rhythms in health and disease. Postgrad. Med. J. *94*, 653–658. https://doi.org/10.1136/postgradmedj-2018-135719.

Kervezee, L., Cermakian, N., and Boivin, D.B. (2019). Individual metabolomic signatures of circadian misalignment during simulated night shifts in humans. PLOS Biol. *17*, e3000303. https://doi.org/10.1371/journal.pbio.3000303.

Kervezee, L., Kosmadopoulos, A., and Boivin, D.B. (2020). Metabolic and cardiovascular consequences of shift work: The role of circadian disruption and sleep disturbances. Eur. J. Neurosci. *51*, 396–412. https://doi.org/10.1111/ejn.14216.

Kessner, D., Chambers, M., Burke, R., Agus, D., and Mallick, P. (2008). ProteoWizard: open source software for rapid proteomics tools development. Bioinformatics *24*, 2534–2536. https://doi.org/10.1093/bioinformatics/btn323.

King, J., Koc, H., Unterkofler, K., Mochalski, P., Kupferthaler, A., Teschl, G., Teschl, S., Hinterhuber, H., and Amann, A. (2010). Physiological modeling of isoprene dynamics in exhaled breath. J. Theor. Biol. *267*, 626–637. https://doi.org/10.1016/j.jtbi.2010.09.028.

King, J., Kupferthaler, A., Frauscher, B., Hackner, H., Unterkofler, K., Teschl, G., Hinterhuber, H., Amann, A., and Högl, B. (2012). Measurement of endogenous acetone and isoprene in exhaled breath during sleep. Physiol. Meas. *33*, 413–428. https://doi.org/10.1088/0967-3334/33/3/413.

Knutson, K.L. (2007). Impact of sleep and sleep loss on glucose homeostasis and appetite regulation. Sleep Med. Clin. *2*, 187–197. https://doi.org/10.1016/j.jsmc.2007.03.004.

Knutson, K.L., and Van Cauter, E. (2008). Associations between sleep loss and increased risk of obesity and diabetes. Ann. N Y Acad. Sci. *1129*, 287–304. https://doi.org/10.1196/annals.1417.033.

Kuznetsova, A., Brockhoff, P.B., and Christensen, R.H.B. (2017). lmerTest Package: Tests in Linear Mixed Effects Models. J. Stat. Softw. *82*, 1–26, 10.18637/jss.v082.i13.

Li, M.D., Li, C.M., and Wang, Z. (2012). The role of circadian clocks in metabolic disease. Yale J. Biol. Med. *85*, 387–401.

Li, S., Park, Y., Duraisingham, S., Strobel, F.H., Khan, N., Soltow, Q.A., Jones, D.P., and Pulendran, B. (2013). Predicting Network Activity from High Throughput Metabolomics. PLoS Comput. Biol. *9*, e1003123. https://doi.org/10.1371/journal.pcbi.1003123.

Longo, N., Frigeni, M., and Pasquali, M. (2016). Carnitine transport and fatty acid oxidation. Biochim. Biophys. Acta *1863*, 2422–2435. https://doi.org/10.1016/j.bbamcr.2016.01.023.

Lütkepohl, H. (2005). Stable vector autoregressive processes. In New Introduction to Multiple Time Series Analysis (Springer Science and Business Media), pp. 13–68.

Mansour, E., Vishinkin, R., Rihet, S., Saliba, W., Fish, F., Sarfati, P., and Haick, H. (2020). Measurement of temperature and relative humidity in exhaled breath. Sens. Actuators B Chem. *304*, 127371. https://doi.org/10.1016/j.snb.2019.127371.

Martinez-Lozano Sinues, P., Tarokh, L., Li, X., Kohler, M., Brown, S.A., Zenobi, R., and Dallmann, R. (2014). Circadian Variation of the Human Metabolome Captured by Real-Time Breath Analysis. PLoS ONE *9*, e114422. https://doi.org/10.1371/journal.pone.0114422.

McCann, M.R., George De la Rosa, M.V., Rosania, G.R., and Stringer, K.A. (2021). L-Carnitine and Acylcarnitines: Mitochondrial Biomarkers for Precision Medicine. Metabolites *11*, 51. https://doi.org/10.3390/metabo11010051.

Miyagawa, T., Kawamura, H., Obuchi, M., Ikesaki, A., Ozaki, A., Tokunaga, K., Inoue, Y., and Honda, M. (2013). Effects of Oral L-Carnitine Administration in Narcolepsy Patients: A Randomized, Double-Blind, Cross-Over and Placebo-Controlled Trial. PLoS ONE *8*, e53707. https://doi.org/10.1371/journal.pone.0053707.

Müller, M., Hernández, M.A.G., Goossens, G.H., Reijnders, D., Holst, J.J., Jocken, J.W.E., van Eijk, H., Canfora, E.E., and Blaak, E.E. (2019). Circulating but not faecal short-chain fatty acids are related to insulin sensitivity, lipolysis and GLP-1 concentrations in humans. Sci. Rep. *9*, 12515. https://doi.org/10.1038/s41598-019-48775-0.

Noya, S.B., Colameo, D., Brüning, F., Spinnler, A., Mircsof, D., Opitz, L., Mann, M., Tyagarajan, S.K., Robles, M.S., and Brown, S.A. (2019). The forebrain synaptic transcriptome is organized by clocks but its proteome is driven by sleep. Science *366*, eaav2642. https://doi.org/10.1126/science.aav2642.

Peters, J., Janzing, D., and Schölkopf, B. (2017). Time Series. In Elements of Causal Inference, J. Peters, D. Janzing, and B. Schölkopf, eds. (MIT press), pp. 197–211.

Petit, J.-M., Burlet-Godinot, S., Magistretti, P.J., and Allaman, I. (2015). Glycogen metabolism and the homeostatic regulation of sleep. Metab. Brain Dis. *30*, 263–279. https://doi.org/10.1007/s11011-014-9629-x.

Redline, S., Kirchner, H.L., Quan, S.F., Gottlieb, D.J., Kapur, V., and Newman, A. (2004). The effects of age, sex, ethnicity, and sleep-disordered breathing on sleep architecture. Arch. Intern. Med. *164*, 406–418. https://doi.org/10.1001/archinte.164.4.406.

Reinke, H., and Asher, G. (2019). Crosstalk between metabolism and circadian clocks. Nat. Rev. Mol. Cell Biol. *20*, 227–241. https://doi.org/10.1038/s41580-018-0096-9.

Rioseras, A.T., Gaugg, M.T., and Martinez-Lozano Sinues, P. (2017). Secondary electrospray ionization proceeds via gas-phase chemical ionization. Anal. Methods *9*, 5052–5057. https://doi.org/10.1039/C7AY01121K.

Robles, M.S., and Mann, M. (2013). Proteomic Approaches in Circadian Biology. In Circadian Clocks, A. Kramer and M. Merrow, eds. (Springer Berlin Heidelberg), pp. 389–407. https://doi.org/10.1007/978-3-642-25950-0_17.

Rodgers, L.C., Cole, J., Rattigan, K.M., Barrett, M.P., Kurian, N., McInnes, I.B., and Goodyear, C.S. (2020). The rheumatoid synovial environment alters fatty acid metabolism in human monocytes and enhances CCL20 secretion. Rheumatology (Oxford) *59*, 869–878. https://doi.org/10.1093/rheumatology/kez378.

Ross, B.M., and Babgi, R. (2017). Volatile compounds in blood headspace and nasal breath. J. Breath Res. *11*, 046001. https://doi.org/10.1088/1752-7163/aa7d10.

Schwarz, E.I., Martinez-Lozano Sinues, P., Bregy, L., Gaisl, T., Garcia Gomez, D., Gaugg, M.T., Suter, Y., Stebler, N., Nussbaumer-Ochsner, Y., Bloch, K.E., et al. (2016). Effects of CPAP therapy withdrawal on exhaled breath pattern in obstructive sleep apnoea. Thorax *71*, 110–117. https://doi.org/10.1136/thoraxjnl-2015-207597.

Seth, A.K., Barrett, A.B., and Barnett, L. (2015). Granger causality analysis in neuroscience and neuroimaging. J. Neurosci. *35*, 3293–3297. https://doi.org/10.1523/JNEUROSCI.4399-14.2015.

Sinues, P.M.-L., Kohler, M., and Zenobi, R. (2013). Monitoring Diurnal Changes in Exhaled Human Breath. Anal. Chem. *85*, 369–373. https://doi.org/10.1021/ac3029097.

Skene, D.J., Skornyakov, E., Chowdhury, N.R., Gajula, R.P., Middleton, B., Satterfield, B.C., Porter, K.I., Van Dongen, H.P.A., and Gaddameedhi, S. (2018). Separation of circadian- and behavior-driven metabolite rhythms in humans provides a window on peripheral oscillators and metabolism. Proc. Natl. Acad. Sci. USA *115*, 7825–7830. https://doi.org/10.1073/pnas.1801183115.

Spörl, F., Korge, S., Jürchott, K., Wunderskirchner, M., Schellenberg, K., Heins, S., Specht, A., Stoll, C., Klemz, R., Maier, B., et al. (2012). Krüppel-like factor 9 is a circadian transcription factor in human epidermis that controls proliferation of keratinocytes. Proc. Natl. Acad. Sci. USA *109*, 10903–10908. https://doi.org/10.1073/pnas.1118641109.

Storey, J.D. (2002). A direct approach to false discovery rates. J. R. Stat. Soc. Series B Stat. Methodol. *64*, 479–498. https://doi.org/10.1111/1467-9868.00346.

Tank, A., et al. (2017). An interpretable and sparse neural network model for nonlinear granger causality discovery. arXiv, 1711.08160. https://arxiv.org/abs/1711.08160.

Tejero Rioseras, A., Singh, K.D., Nowak, N., Gaugg, M.T., Bruderer, T., Zenobi, R., and Sinues, P.M. (2018). Real-Time Monitoring of Tricarboxylic Acid Metabolites in Exhaled Breath. Anal. Chem. *90*, 6453–6460. https://doi.org/10.1021/acs.analchem.7b04600.

Tsugawa, H. (2019). MS-DIAL. http://prime.psc.riken.jp/compms/msdial/main.html#MSP.

Tsugawa, H., Cajka, T., Kind, T., Ma, Y., Higgins, B., Ikeda, K., Kanazawa, M., VanderGheynst, J., Fiehn, O., and Arita, M. (2015). MS-DIAL: data-independent MS/MS deconvolution for comprehensive metabolome analysis. Nat. Methods *12*, 523–526. https://doi.org/10.1038/nmeth.3393.

Van Cauter, E., Polonsky, K.S., and Scheen, A.J. (1997). Roles of circadian rhythmicity and sleep in human glucose regulation. Endocr. Rev. *18*, 716–738. https://doi.org/10.1210/edrv.18.5.0317.

Williams, N.C., and O'Neill, L.A.J. (2018). A Role for the Krebs Cycle Intermediate Citrate in Metabolic Reprogramming in Innate Immunity and Inflammation. Front. Immunol. *9*, 141. https://doi.org/10.3389/fimmu.2018.00141.

Winkler, I., Panknin, D., Bartz, D., Müller, K.-R., and Haufe, S. (2016). Validity of Time Reversal for Testing Granger Causality. IEEE Trans. Signal Process. *64*, 2746–2760. https://doi.org/10.1109/TSP.2016.2531628.

Zhao, S., Feng, X.F., Huang, T., Luo, H.H., Chen, J.X., Zeng, J., Gu, M., Li, J., Sun, X.Y., Sun, D., et al. (2020). The Association Between Acylcarnitine Metabolites and Cardiovascular Disease in Chinese Patients With Type 2 Diabetes Mellitus. Front. Endocrinol. (Lausanne) *11*, 212. https://doi.org/10.3389/fendo.2020.00212.

Zou, H., and Hastie, T. (2005). Regularization and variable selection via the elastic net. J. R. Stat. Soc. Series B Stat. Methodol. *67*, 301–320. https://doi.org/10.1111/j.1467-9868.2005.00503.x.

STAR★METHODS

KEY RESOURCES TABLE

Reagent or resource	Source	Identifier
Deposited data		
Raw data	This paper	ETH research collection: https://doi.org/10.3929/ethz-b-000422459
Software and algorithms		
Code for data analysis	This paper	ETH research collection: https://doi.org/10.3929/ethz-b-000422459

RESOURCE AVAILABILITY

Lead contact

Further information and requests should be directed to and will be fulfilled by the lead contact, Malcolm Kohler (malcolm.kohler@usz.ch).

Materials availability

This study did not generate new unique reagents.

Data and code availability

- All original data used in this publication are made available in a curated data archive at ETH Zurich (https://www.research-collection.ethz.ch): ETH research collection: https://doi.org/10.3929/ethz-b-000422459. The DOI is also listed in the key resources table.
- The original code used in this publication is made available in a curated data archive at ETH Zurich (https://www.research-collection.ethz.ch): ETH research collection: https://doi.org/10.3929/ethz-b-000422459. The DOI is also listed in the key resources table.
- Any additional information required to reanalyze the data reported in this paper is available from the lead contact upon request.

EXPERIMENTAL MODEL AND SUBJECT DETAILS

Sleep experiment

Study participants

A group of 14 healthy volunteers (12 non-smokers, 1 ex-smoker, 1 active smoker) in the age of 29.2 ± 8.3 years was recruited for this study. Participant characteristics are summarized in Table 1. 57% of the study subjects were male and mean BMI ± SD was 22 ± 3 kg/m^2. They did not take any medication. The participants were asked to refrain from eating, drinking (except water), chewing gum, brushing their teeth and using any facial cosmetics (such as lip balm) during at least one hour prior to the measurements. Each individual spent two consecutive nights in the laboratory. In the first night, SESI-HRMS measurements were carried out in positive ionization mode, in the second night in negative ionization mode. A full polysomnography was performed in both nights. One participant could not be measured due to dysfunction of the MS and one quit the study after the first night. Therefore, the final numbers of included participants are n = 13 for measurements in positive ion mode and n = 12 for measurements in negative ion mode. The measurements were conducted in accordance with the Declaration of Helsinki and written informed consent was obtained from all participants. The study was approved by the local ethical committee (KEK-ZH 2016-00384).

Blood-breath comparison experiments

Study participants

Nine healthy volunteers in the age of 30.6 ± 7.8 years, 44% female, were studied to compare metabolite levels in breath and blood. All participants were non-smokers and did not take any medication. The participants underwent real-time breath analysis by SESI-HRMS and whole blood has been withdrawn simultaneously. Participants were asked to refrain from eating, drinking (except water), chewing gum, brushing their teeth and using any facial cosmetics (such as lip balm) during at least one hour prior to the measurements. The experiments were conducted in accordance with the Declaration of Helsinki and written informed consent was obtained from all participants. The study was approved by the local ethical committee (KEK-ZH 2016-00384).

METHOD DETAILS

SESI-HRMS measurements during sleep

In order to sample exhaled breath continuously, we modified a continuous positive airway pressure (CPAP) mask with a hole (inner Ø = 12 mm), through which the individuals could inhale and exhale freely (Figure 1A). 0.2 L/min were drawn into the ionization chamber by a vacuum pump installed at the exhaust of the ionization source. The flow was controlled by a mass flow controller. The mask was connected to the SESI source via a flexible stainless steel tube, which was coated with SilcoNert 2000 (SilcoTek GmbH, Bad Homburg, Germany) and heated to 130°C in order to prevent adsorption and condensation. The flexibility of this tube allowed the participants to move and sleep in different body positions. Real-time breath analysis was performed with a commercial SESI source (SEADM, Spain) coupled to a TripleTOF 5600+ high resolution mass spectrometer (AB Sciex, Concord, ON, Canada). The spray solution consisted of 0.2% formic acid (99%–100%, VWR chemicals) in water (LC-MS grade, Fisher Scientific) and a voltage of 5.5 kV was applied in positive ion mode and −4.5 kV in negative mode. Full scan mass spectra were recorded with an accumulation time of 10 s in a mass range from 50 to 500 Da in positive mode and 50 to 450 Da in negative ion mode respectively. The ion source was heated to 130°C, curtain gas was set to 10, collision gas was set to 0, collision energy to (-)10 eV, declustering potential (-)20 V

Polysomnography

In parallel to the SESI-HRMS measurements full polysomnography was performed in all participants using an Alice 6 system (Philips Respironics, PA USA). For the setup as well as the scoring the recommendations from the American Academy of Sleep Medicine from 2007 were applied (Iber, 2007).

Blood breath comparison experiments

Real-time SESI-HRMS breath analysis

Real-time breath measurements were preformed similar to breath measurements during sleep. Instead of the flexible tube and the mask a single-use mouthpiece was connected to the sampling line. The flow through the ion source was controlled to 0.2 L/min by a low-Δp mass flow controller (Bronkhorst, Switzerland) at the exhaust of the source. The participants were exhaling with a pressure drop of 12 mbar and to enable sampling of end-tidal breath, a flow-splitter was installed front-end. No vacuum pump was used in this setup. Full scan mass spectra were recorded in the range of 50 to 500 Da in positive mode with an accumulation time of 1 s. At least six exhalations were measured per person. All other parameters were as described for the measurements during sleep.

UPLC-tandem-MS measurements of serum

Whole blood was left at room temperature for 10-30 min for clotting. To obtain serum, it was then centrifuged for 15 min at 1500 rpm. Aliquots of 200 μL were taken, 200 μL of 1 mg/mL $^{15}N_2$-tryptophan (Cambridge Isotope Laboratories, Inc., Tewksbury, USA) in water were added as internal standard and proteins were precipitated by the addition of 600 mL of methanol (LC-MS grade, Fisher Scientific, Pittsburgh, USA). Samples were incubated on ice for 10 minutes and centrifuged at 4°C and 15800 g for 15 min. The supernatant was filtered using a 0.2 μm reversed cellulose membrane filter, 400 μL were aliquoted and solvents were removed in a vacuum dryer. The residual was resuspended in 75 mL of a mixture of water and methanol (95/5, v/v, both LC-MS grade, Fisher Scientific, Pittsburgh, USA), sonicated (10 min) and centrifuged (15 min, 15800 g) and transferred to LC vials with glass inserts. 10 μL were injected for analysis. One sample per person has been analyzed, analytical reproducibility was verified with quality control samples.

Chromatographic separation was performed on an ACQUITY UPLC system (I-Class, Waters, MA, USA) using an ACQUITY UPLC BEH C18 column (1.7 μm, 2.1 × 150 mm, Waters) with a corresponding precolumn filter. The flow rate was set to 240 μL/min using a binary mixture of solvent A (water with 0.5% methanol and 0.1% formic acid) and solvent B (methanol with 0.1% formic acid). The following gradient was used: 5% B (1 min), 5 to 95% B (9 min), 100% B (2 min), and 5% B (2 min). The column temperature was set to 30°C and the autosampler was kept at 5°C.

Mass spectra were recorded on a quadrupole-time-of-flight high resolution mass spectrometer (TripleTOF 5600+, AB Sciex, Concord, ON, Canada) with a heated electrospray ionization source in positive ion mode. Full-scan mass spectra (m/z range 50 to 650 Da) and data dependent MS-MS acquisitions (m/z range 50 to 650 Da) were performed. Curtain gas was set to 30, GS1 and GS2 were set to 50, a spray voltage of 5 kV was applied and the ion source was heated to 500°C. The total cycle time was kept at 800 ms to obtain at least 12 points/peak (minimal LC peak width = 9 s) with 150 ms for full scan MS and 85 ms for seven product ion scans acquired with a collision energy of 10/20/30 eV.

QUANTIFICATION AND STATISTICAL ANALYSIS

Data preprocessing

Raw mass spectra were converted into .mzXML format using MSConvert (ProteoWizard) (Kessner et al., 2008) and polysomnography data was exported to .edf files. Further data processing was performed in MATLAB R2018b, R 3.6.1 and python 3.7.1. First, mass spectra were aligned across all scans and all subjects. Then, a peaklist was generated by interpolation and averaging every 50th scan of all spectra. For positive ion mode spectra, the obtained peaklist was recalibrated with a list of known reference peaks. All peaks were centroided by integration yielding time traces of all peaks (1458 in positive ion mode, 1028 in negative ion mode) for each sub-

Algorithm 1. Bootstrapping procedure for discovering metabolites with Granger causal associations with sleep stages

Input: N replicates of target $\{Y_t\}_{t=1}^{T}$ and predictors $\{X^j\}_{t=1}^{T}$, for $j = 1,\ldots,p-1$; maximum lag $K \in \mathbb{N}$; regularization parameter $\lambda > 0$; parameter $\alpha \in [0, 1]$; threshold $c_{th} > 0$; confidence level $\gamma \in (0, 1)$; number of re-samples $B \in \mathbb{N}$.
Output: Set $\widehat{S}$ of predictors that Granger-cause Y.
$\widehat{S} \leftarrow \{\}$
for $b = 1$ *to* B **do**
  Sample $\boldsymbol{N}$ replicates $\boldsymbol{I}^b = \{i_1^b, \ldots, i_N^b\}$ with replacement from $\boldsymbol{I} = \{\mathbf{1}, \ldots, \boldsymbol{N}\}$.
  Train the neural network on replicates in $\boldsymbol{I}^b$ with parameters $\boldsymbol{K}$, λ and α using mini-batch gradient descent.
  Retrieve absolute values of importance weights $\boldsymbol{c}_1^{*b}, \boldsymbol{c}_2^{*b}, \ldots, \boldsymbol{c}_{p-1}^{*b}$ from the trained model.
end
for $j = 1$ *to* $p - 1$ **do**
  Compute the empirical $(\mathbf{1} - \gamma)$-quantile of bootstrapped weights for the j-th variable $\boldsymbol{q}_j := \boldsymbol{q}_{\boldsymbol{c}_j^*}(\mathbf{1} - \gamma)$.
if $q_j \geq c_{th}$ **then**
  $\widehat{\boldsymbol{S}} \leftarrow \widehat{\boldsymbol{S}} \cup \{j\}$
end
return $\widehat{S}$

ject. In order to reduce the number of features, the following filtering criteria were applied: Only features that were higher in exhaled breath than dry room air in at least 50% of the subjects were kept. Further, features with median intensities below 30 counts per second in at least 50% of the subjects were removed. Since sleep stages have been determined from PSG in 30 s intervals and mass spectra were recorded every 10 s, thus we interpolated sleep stage information, i. e. we always attributed the previous sleep stage measured. MS time traces were smoothed by Savitzky Golay filtering (smoothing window of 19 data points). In order to reduce technical noise, such as spray instabilities, but also to account for breathing variations, we normalized our data. The humidity of breath is supposed to be constant (Burton, 2000). Therefore, we used the water cluster signal ($[(H_2O)_3+H]^+$, m/z 55.03897) for normalization in positive ion mode and the signal of a water-formic acid cluster ($[HCOOH+H_2O]^-$, m/z 63.00877) for normalization in negative ion mode. The water signal varied across the night and across individuals (Data S3). Recently, significant inter-individual differences in relative humidity of human breath have been reported from heterogeneous cohorts (Mansour et al., 2020). Our normalization might therefore introduce a bias here. However, we lack of any better method to distinguish between biological and technical noise. MS times and PSG times were synchronized, data points during lights on period as well as data points, where only MS or only PSG data was available, were removed. Moreover, very short sleep stages (< 70 s) were annotated with the previous one.

Statistics

Detrending

In order to separate gradual changes in metabolic profiles across the night from acute changes across sleep stages, we subtracted a baseline prior to statistical analysis, which we obtained from Savitzky-Golay filtering (smoothing window of 1001 datapoints).

One-way ANOVA

We fitted our data for each metabolite with linear mixed effects models with a fixed effect for sleep stage and a random effect for person using the Satterthwaite's degrees of freedom method (Kuznetsova et al., 2017). We then performed an χ^2 test to assess, whether the model with the different levels for the different sleep stages performs better than the simplest model with only an intercept. The obtained p values were corrected for multiple hypothesis testing using Storey's procedure (Storey, 2002).

Pairwise comparisons

In order to perform summary statistics, we binned our data sleep stage-wise, by averaging all spectra corresponding to one sleep stage for each subject. We then performed pairwise comparisons of the different sleep stages using a two-sided Wilcoxon signed ranked test. Again, we corrected for multiple hypothesis testing using Storey's procedure (Storey, 2002). In addition, we calculated pairwise effect sizes (Cohen's d (Cohen, 1977)) between sleep stages for each metabolite.

Inferring non-linear Granger causality with neural networks

To discover metabolic features that are Granger-caused by different sleep stages, we trained feedforward neural networks with a specially tailored architecture (see Figure S1, code publicly available, ETH research collection: https://doi.org/10.3929/ethz-b-000422459) with sparsity-inducing penalty terms in the loss function. After the above mentioned preprocessing, we performed training on positive and negative mode MS time series (non-binned) for three stages of sleep separately: wakefulness, N3 and REM. All sequences were time-reversed (Winkler et al., 2016) to infer Granger causal relationships *from* sleep stage transitions to metabolism. We used a bootstrap procedure (Fox, 2002) to identify significant interactions between variables (see Algorithm 1). Implementation details, values of hyperparameters and the results of simulation experiments and cross-validation are provided in the following paragraphs.

The Granger causality approach that we adopt has seen few applications in the analysis of time course MS data. This method has several advantages over conventional approaches, such as correlation analysis and analysis of variance (ANOVA):

- It can represent non-additive nonlinear dependencies between sleep stage labels and multiple mass spectrometric features;
- It deals with time series in a principled way and can account for time-delayed (auto)regressive relationships;
- Granger causality is a directed relationship, whereas (cross-)correlation does not focus on precedence in time;
- It does not merely examine marginal relationships, it performs multiple regression.

More formally, when inferring Granger causality, we consider the following setting. We assume that we are given N replicates of MS and sleep stage time series retrieved from N different subjects. These time series include:

- A categorically-valued sleep stage time series $\{\boldsymbol{Y}_t\}_{t=1}^{T}, \boldsymbol{Y}_t \in \{\boldsymbol{W}, \boldsymbol{N}_1, \boldsymbol{N}_2, \boldsymbol{N}_3, \boldsymbol{R}\}$, for each $\boldsymbol{t}$;
- M continuously-valued time series $\{\boldsymbol{X}_t^j\}_{t=1}^{T}$, where $\boldsymbol{j} = \boldsymbol{1}, \ldots, \boldsymbol{p}-\boldsymbol{1}$, and $\boldsymbol{X}_t^j$ corresponds to the relative intensity of ion $\boldsymbol{j}$ in the mass spectrum of exhaled breath at time step $\boldsymbol{t}$.

Our goal is then to identify metabolites that are causally related to sleep stages, i.e., metabolites that drive the sleep stage, denoted by $X^j \to Y$, and metabolites that are driven by the stage, $Y \to X^j$.

Granger causality

Granger causality, introduced by C. W. J. Granger (Granger, 1969) is one of the most popular approaches to practical causal time series analysis. Intuitively, if time series X is a cause of Y, then the past of X should be useful for predicting the future of Y (Eichler, 2012). Formally, Granger causality from stationary time series $\{X_t\}_{t\in\mathbb{Z}}$ to $\{Y_t\}_{t\in\mathbb{Z}}$ can be defined as follows (Eichler, 2012). Let $\mathcal{I}^*(t-1)$ be an information set containing all information available in the universe up to time $t-1$, and let $\mathcal{I}^*_{-X}(t-1)$ be the same set as $\mathcal{I}^*(t-1)$, but with values of time series X removed (up to time $t-1$). We say that X Granger-causes Y if and only if Y_t and $\mathcal{I}^*(t-1)$ are not conditionally independent given $\mathcal{I}^*_{-X}(t-1)$, for all $t\in\mathbb{Z}$. This definition for the bivariate case can be easily extended to multivariate time series. In practice, Granger causality is often inferred by assuming some time series model, for, instance, vector autoregression (VAR). It can be shown that in VAR Granger causality can be determined from zero constraints on the coefficients (Lütkepohl, 2005). Although simple and interpretable, such representation does not allow for nonlinearities and complex interactions between variables. Therefore, we leverage highly expressive neural networks (NN) (Goodfellow et al., 2016) to infer Granger causality.

Limitations of Granger causality

While the concept of Granger causality is practically compelling, it has some shortcomings and can be misleading in certain cases. Granger causality analysis can yield spurious conclusions if the set of considered variables is not *causally sufficient* (Peters et al., 2017). For example, if there exist "superior" mechanisms that regulate both metabolism and sleep, statements of causality between ion intensities and sleep phases could be meaningless. (Such superior mechanisms would be biologically logical to imagine.) Issues can also arise if time series are not sampled frequently enough to recover relationships (unlikely in our case) or if there exist instantaneous interactions between variables, which are imaginable in biochemical pathways (Peters et al., 2017).

Model

Inspired by componentwise multilayer perceptron (cMLP) (Tank et al., 2017), we introduce our own feedforward NN architecture for *unsupervised* Granger causal discovery. For the sake of convenience, we refer to it as Granger causal multilayer perceptron (GC-MLP). Data S4 depicts the schematic of a GC-MLP. This network is trained in a *supervised* manner to forecast target time series Y based on past K values of predictors $X^1, X^2, \ldots, X^{p-1}$ and Y itself. Note, that the network consists of p disjoint encoders which produce "hidden" representations for each variable. These representations are then multiplied with *importance weights* $c_1, c_2, \ldots, c_p$ and concatenated into one vector.

Consequently, this vector is fed into a multilayer perceptron (MLP) to compute forecast $\widehat{\boldsymbol{y}}_t$ of Y_t. Granger causality from X^j to Y can then be identified by inspecting importance weight c_j. Ideally, we expect that $|c_j| \approx 0$ when $X^j \not\to Y$, and $|c_j| > 0$ when $X^j \to Y$. The loss function of GC-MLP is crucial for estimating Granger causality. It encourages importance weights to be sparse by using an elastic-net-style (Zou and Hastie, 2005) term that penalizes ℓ_1 and ℓ_2 norms of $\boldsymbol{c} = [c_1 \quad \ldots \quad c_p]$:

$$-\sum_{t=K+1}^{T}\sum_{j=1}^{C}\gamma_j\left\{(\boldsymbol{y}_t)_j \ln\left((\widehat{\boldsymbol{y}}_t)_j\right) + \left(1-(\boldsymbol{y}_t)_j\right)\ln\left(1-(\widehat{\boldsymbol{y}}_t)_j\right)\right\} + \lambda\left(\alpha||\boldsymbol{c}||_1 + (1-\alpha)\left|\left|\boldsymbol{c}\right|\right|_2^2\right),$$

where K is the maximum lag of autoregressive relationships; C is the number of classes; γ_j is the weight for class j; $\widehat{\boldsymbol{y}}_t$ refers to the forecast for the value of $\boldsymbol{y}_t$; $(\boldsymbol{v})_j$ stands for the j-th component of vector $\boldsymbol{v}$; $\lambda > 0$ is the regularization parameter; and $\alpha \in [0, 1]$ controls the tradeoff between ℓ_1 and ℓ_2 penalties. Note that herein $\boldsymbol{y}_t$ is assumed to be categorical and encoded with the one-hot encoding scheme.

Bootstrapping

In order to quantify our uncertainty about Granger causal relationships (i.e., to infer a conventional p value), we leverage bootstrapping (Fox, 2002). Many GC-MLPs are trained on resampled time series replicates to construct a confidence interval for each c_j that can be used to decide whether relationship $X_j \rightarrow Y$ is significant. The full procedure is summarized in Algorithm 1.

Time reversal

Algorithm 1 identifies a set of Granger causes of response variable Y. We might be interested in solving the inverse problem: finding a set of predictors Granger-caused by the response. The naive solution would be to train a GC-MLP for each predictor variable X^j as the response and identify if Y Granger-causes X^j. In high-dimensional mass spectrometric time series, this approach is prohibitively costly. We can leverage time-reversed Granger causality (Winkler et al., 2016) by performing inference on time-reversed sequences. Intuitively, we expect that, if $Y \rightarrow X^j$, then the future values of X^j should be useful for predicting the past values of Y. Thus, instead of naively training $p - 1$ models, with time reversal we only need one GC-MLP.

Hyperparameters and network specification

We implemented the model in Python programming language (version 3.7.1) using PyTorch machine learning library (version 1.0.1) We considered (auto-)regressive relationships up to lag $K = 30$ ($\approx$300 s). We choose the model order sufficiently large, to avoid potential misspecification. Each GC-MLP had 100 hidden units in each encoder and 200 shared hidden units. We set the regularization parameter λ to 0.001 and $\alpha = 0.8$. The choice of λ is motivated by simulation experiment results discussed below. In the cross-entropy loss, the weight of 0.9 is assigned to the less prevalent sleep stage, whereas the weight of 0.1 is assigned to the more prevalent one. The training is performed for one epoch by gradient descent using Adam optimizer with mini-batches of 100 data points. For the bootstrapping procedure, we trained $B = 1000$ models and used parameter values $c_{th} = 0.0025$ and $\gamma = 0.95$.

Cross-validation

To investigate whether it is possible to predict sleep stages solely based on mass spectrometric profiles, we performed cross-validation. Granger causal discoveries discussed before would be meaningless, if trained neural networks possessed no predictive power. During validation we did not include sleep stage time series as a predictor. We used the leave-one-subject-out cross-validation (CV) procedure to see how well GC-MLPs generalize across different subjects. Namely, for each iteration, we left out one subject and trained a neural network on the rest. To evaluate performance, we employed the balanced accuracy score. This metric is more appropriate than the normal accuracy because of imbalances in frequencies of classes. Average balanced accuracy CV scores are shown in Table S2A and S2B. For all responses, mean scores are significantly greater-than 0.5 ($\alpha = 0.05$). Thus, on average, in all prediction tasks GC-MLPs perform better than the random classifier. To sum up, the results of cross-validation suggest that there might be some structure in the data driven by differences between stages of sleep.

Simulation experiments

We performed experiments on perturbed mass spectrometry data to verify that our neural network technique for discovering Granger causality behaves as expected. We explored the number of false discoveries made in different scenarios and investigated the relationship between the number of false discoveries and regularization parameter λ. Note that in these experiments we did not reverse the time series.

First, we examine inference results under permuted ion intensity time series. We considered five features that had been originally discovered as Granger-causing REM sleep stage transitions with mass-to charge ratios 69.070, 118.065, 152.128 229.252 and 271.299. We generated 10 synthetic datasets wherein we randomly permuted all metabolic time series except for the sequences of these five variables (10 random seeds used). Subsequently, we applied the bootstrapping procedure on these datasets with $B = 100$ resamples. We expect that none of the variables the time series of which were permuted are identified as causal, whereas the five features that remain fixed should be. In all simulations, every of the invariant variables is discovered as causal. Moreover, none of the permuted time series are falsely claimed to drive the response.

Another experiment we performed was with randomly permuting REM sleep stage labels while keeping metabolic time series untouched. In this setting, we expect our inference technique to identify no variables that are causally related with the permuted target. We ran the bootstrapping procedure on 10 different simulated datasets with $B = 100$ resamples. In all datasets, no spurious relationships were found from predictors to the target.

Finally, we replaced the original REM signal with a synthetic target time series that behaves like a sleep stage sequence. Similarly to the setting above, we expect no causal links to be inferred. We performed bootstrapping on 10 simulated datasets with $B = 100$ resamples. We ran the inference for $\lambda = 0, 10^{-4}, 10^{-3}, 10^{-2}$. Table S2C contains numbers of false discoveries made by the inference technique under different values of λ. Observe that for the largest value almost no false discoveries are made. A decrease in the value of the regularization parameter seems to lead to more spurious causal relationships being inferred. For $\lambda = 0.001$, the value we used in the causal analysis of MS and sleep stage time series, on average, 14.4 false discoveries are made. Although this result is not ideal, larger values of the regularization parameter could be, in practice, too conservative and, thus, may lead to inferring a causal graph that is much sparser than the true structure, i.e., the loss of power.

In general, the results of the simulation experiments are promising. The inference technique we proposed behaves as expected on perturbed MS data; and we can adequately control the number of false discoveries with parameter λ.

Pathway enrichment analysis and compound ID

Automated compound information using metabolic pathway information was performed using the mummichog algorithm (Li et al., 2013; Chong et al, 2019). The algorithm was run with the q-values obtained from pairwise comparisons described above. Significance threshold was set to q = 0.05 and the manually curated human genome-scale metabolic model from the mummichog python package ("MFN") was used as pathway library. Adducts were restricted to $[M+H]^+$ and $[M-H]^-$. Since mostly protonated or deprotonated species are formed in SESI (Rioseras et al., 2017), we removed all radicals from the list of annotated compounds. We did further manual investigation on metabolites involved in the pathways with the highest numbers of significant hits and we thus reduced the selection to a few key pathways. We selected only pathways with very high metabolite coverage and pathways, in which key metabolites were significant hits. Carboxylic acids, where protonated species were significant hits, but not the deprotonated forms, were neglected. When pathway coverage was only high, because one mass resulted in several significant hits due to different isomers in one pathway, those were also ignored. For compounds involved in those pathways of interest, MS-MS spectra obtained from exhaled breath condensate (EBC) were compared to database spectra. Experimental details of EBC collection and ultra-high performance liquid chromatography-tandem MS methods are described elsewhere (Gaugg et al., 2017). If features were not detected in EBC, real-time SESI-MS-MS spectra were recorded using an Orbitrap QExactive Plus mass spectrometer (Thermo Fisher, Germany) with a commercial SESI source (SuperSESI, Fossil Ion Tech, Spain). Breath was sampled at 0.3 L/min. The sampling line of the ion source was heated to 130°C, the ionization chamber was heated to 90°C and a spray solution of 0.1% formic acid in water was used. A spray voltage of (-)3500 V was applied. The mass spectrometer was operated at 140,000 resolution in data dependent acquisition mode with an isolation window of 0.4 m/z. The automated gain control was set to 1e6 at MS1 level and to 1e5 at MS-MS level and a maximal injection time of 500ms was used. MS-MS library spectra were obtained from the spectral library with all publicly available MS-MS records available for MSDial (Tsugawa et al., 2015; Tsugawa, 2019).

Blood-breath comparison experiments

Data analysis

Data preprocessing of breath spectra was performed as described elsewhere (Gaugg et al., 2019). Signal intensities were normalized to the water cluster signal ($[(H_2O)_3+H]^+$, m/z 55.03897). Raw data obtained from blood was converted to .mzXML format with MSConvert (ProteoWizard) (Kessner et al., 2008) and further processed in MATLAB R2018b, R 3.6.1. After centroiding, chromatographic peaks of target compounds were integrated. Robust linear regression (Holland and Welsch, 1977) was performed with the intensities obtained from blood and breath. In addition, we calculated Pearson's and Spearman's correlation coefficients. As described above, we compared MS-MS spectra from blood and exhaled breath condensate with database spectra, to confirm the identities of the detected acylcarnitines.